Synthesis and Antibacterial Activity of Rhodanine-Based Azo Dyes and Their Use as Spectrophotometric Chemosensor for Fe^{3+} Ions

Dana Akram [1], Ismail A. Elhaty [2],* and Shaikha S. AlNeyadi [1],*

[1] Department of Chemistry, College of Science, UAE University, P.O. Box 15551, Al-Ain, UAE; 201450261@uaeu.ac.ae
[2] Department of Nutrition and Dietetics, School of Health Sciences, Istanbul Gelisim University, Istanbul 34310, Turkey
* Correspondence: iaeismail@gelisim.edu.tr (I.A.E.); shaikha.alneyadi@uaeu.ac.ae (S.S.A.);
    Tel.: +009-0212-422-70-00 (I.A.E.); +009-7137-136-132 (S.S.A.)

check for updates

Abstract: This research includes the design and synthesis of new derivatives for rhodanine azo compounds (**4a–c**) containing a naphthalene ring. Physiochemical properties of the synthesized compounds were determined by their melting points, FTIR, ^{1}H-NMR, ^{13}C-NMR, and elemental analysis spectroscopic techniques. The biological activities of the newly prepared azo rhodanine compounds were evaluated against some pathogenic bacteria using three different bacterial species including (*Escherichia coli.*, *Pseudomonas aeruginosa*, *Staphylococcus aureus*) and compared with amoxicillin as a reference drug. The results showed that our compounds have moderate-to-good vital activity against the mentioned pathogenic bacteria. The selectivity and sensitivity of the newly prepared rhodanine azo compounds with transition metals Co^{2+}, Cu^{2+}, Zn^{2+}, Ni^{2+}, and Fe^{3+} were studied using UV–vis and fluorescence spectroscopy techniques. Among the synthesized azos, azo **4c** showed affinity toward Fe^{3+} ions with an association constant of 4.63×10^8 M^{-1}. Furthermore, this azo showed high sensitivity toward Fe^{3+} ions with detection limits of 5.14 μM. The molar ratio and Benesi–Hildebrand methods confirmed the formation of complexes between azo **4c** and Fe^{3+} with 1:2 binding stoichiometry. Therefore, azo **4c** showed excellent potential for developing efficient Fe^{3+} chemosensors.

Keywords: fluorescence; synthesis; rhodanine; Fe^{3+} sensing; UV/vis spectrometry

1. Introduction

Chemosensors have received considerable attention due to their recognition of heavy-metal ions and importance in several disciplines such as clinics, biochemistry, and environment [1]. Therefore, the development of efficient sensors for the detection of metal ions is one of the most active research areas in the chemical sciences because of their simplicity, low cost, local observation, sensitive ion-induced spectroscopic changes, and real-time examination of the metal-ion content [2–4].

Azo dyes are a wide class of synthetic organic dyes and have been widely used in dye chemistry [5]. Numerous heterocyclic azo dyes have been used in the textile industry and medicinal applications such as photodynamic therapy, antiviral, antifungal, and antioxidant properties [6,7]. Rhodanine derivatives, a class of heterocyclic compounds, are used in colorimetric sensors, fluorescent dyes, and pharmacological studies [8]. Rhodanine-based azo compounds can interact quite easily with metal ions through the heteroatoms (S, N, and O) present in their structures. These compounds can chelate with a large number of metal ions, as they form a stable six-membered ring after complexation with a metal ion.

Iron ions are one of the most essential trace elements in the human body. The participation of these ions is very important for many physiological processes including oxygen transportation, oxygen metabolism, transcriptional regulation, and electron transfer [9]. Detecting Fe^{3+} is of great importance, therefore, great efforts have been devoted to developing sensors for the detection of Fe^{3+} with sensitivity and selectivity. However, most of the reported Fe^{3+} probes have several limits such as poor selectivity to Fe^{3+} and only a few probes have been applied in biological systems [10]. Several methods have been developed to detect Fe^{3+}, including atomic absorption spectroscopy [11], colorimetric analysis [12,13], mass spectrometry [14], electrochemical analysis [15], and fluorescence spectroscopic analysis [16]. In the present paper, we report the synthesis of 5-naphthylazorhodanine derivatives with the potential to act as selective chemosensors for one of the following metal ions; Co^{2+}, Cu^{2+}, Zn^{2+}, Ni^{2+}, and Fe^{3+} using UV/vis and fluorescence spectroscopic techniques. The synthesized rhodanine azo compounds were also screened for their antibacterial activity.

2. Material and Methods

2.1. Chemistry

All chemicals, reagents, and solvents were obtained from Sigma-Aldrich and utilized without further purification. The reactions' progress was monitored using thin-layer chromatography (TLC) on silica gel glass plates (Silica gel, 60 F_{254}, Fluka), and a UV lamp was used to visualize the spots. The products were purified using column chromatography on silica gel S (0.063–0.1 mm). A Gallenkamp apparatus was used to measure the melting points and recorded without correction. Infrared spectra were recorded on Thermo Nicolet model 470 FT-IR spectrophotometer using KBr pellets between 4000 and 500 cm^{-1}. ^1H and ^{13}C-NMR spectra were recorded in DMSO-d_6 and $CDCl_3$ solutions and tetramethylsilane (TMS) as an internal reference using 400 MHz Varian instruments. A Leco Model CHN-600 elemental analyzer was used to conduct the elemental analysis. UV–vis absorption spectra were obtained using a Cary 50 UV–vis spectrophotometer supported by 1.0 cm quartz cells (Varian, Austria). Fluorescence measurements were conducted inside quartz cells using a Cary Eclipse model-3 spectrofluorometer equipped with a high-intensity xenon flash lamp and 1.0 cm path length (Varian, Austria).

2.2. Synthesis of Rhodanine Azos **4a–c**

2.2.1. General Procedure

Twenty-five milliliters of aqueous hydrochloric acid solution (12 M, 32.19 mmol) was added to 2-aminonapthalene (**1**) (5 mmol). Sodium nitrite solution (5.1 mmol, in 10 mL of water) was added dropwise over 10 min to the cooled (0 °C) and stirred mixture. The formed diazonium chloride (**2**) was maintained at 0–5 °C, then a 25 mL ethanolic solution of 2-thioxo-4-thiazolidinone (**3**) (5 mmol) containing sodium acetate (5 mmol) was added dropwise over 20 min. The produced slurry mixture was allowed to stir for 2 h at 5 °C then it was left to stand overnight. The resulted dark red precipitate was filtered by washing with water several times. The crude azo dye was recrystallized from hot ethanol giving (**4**) in a good yield.

2.2.2. (E)-3-Amino-5-(Naphthalen-2-Yldiazenyl)-2-Thioxothiazolidin-4-One (**4a**)

Dark red; yield 81%; mp 245 °C; R_f 0.50; IR(KBr, cm^{-1}): 3435 (NH_2), 3026 (C–H aromatic), 1700 (C=O), 1629 (C=C), 1468 (N=N), 1246 (C=S); ^1H-NMR [DMSO-d_6, 400 MHz]: 3.35 (s, 1H, CH), 5.90 (brs, 2H, NH_2, exchanges with D_2O), 7.37–7.93 (m, 7H, aromatic-H); ^{13}C-NMR [DMSO-d_6, 100 MHz]: 110.3 (C5-rhodanine), 116.1 (C3-naphthalene), 121.9 (C1-naphthalene), 124.9 (C7-naphthalene), 127.4 (C6-naphthalene), 127.6 (C4- naphthalene), 128.2 (C8-naphthalene), 129.9 (C5-naphthalene), 130.3 (C4a-naphthalene), 134.1 (C8a-naphthalene), 141.0 (C2-naphthalene), 159.6 (C=O), 184.9 (C=S); Anal.

Calcd. for $C_{13}H_{10}N_4OS_2$: C, 51.64; H, 3.33; N, 18.53; O, 5.29; S, 21.21; Found: C, 52.04; H, 3.63; N, 18.73; S, 21.51.

2.2.3. (E)-2-(5-(Naphthalen-2-Yldiazenyl)-4-Oxo-2-Thioxothiazolidin-3-Yl)Acetic Acid (4b)

Dark brown; yield 89%; mp 130 °C; R_f 0.30; IR(KBr, cm^{-1}): 3427 (OH, COOH), 3060 (C–H aromatic), 2925 (C–H aliphatic), 1720 (C=O), 1630 (C=C), 1403 (N=N), 1287 (C=S); ^{1}H-NMR [DMSO-d_6, 400 MHz]: 3.41 (brs, 1H, CH), 4.74 (s, 2H, CH_2), 7.36–8.79 (m, 7H, aromatic-H), 11.69 (brs, 1H, OH, exchanges with D_2O); ^{13}C-NMR [DMSO-d_6,100 MHz]: δ, ppm) 45.3 (CH_2), 110.5 (C5-rhodanine), 116.2 (C3-naphthalene), 122.3 (C1-naphthalene), 125.0 (C7-naphthalene), 126.4 (C6-naphthalene), 127.6 (C4-naphthalene), 130.3 (C8-naphthalene), 134.0 (C5-naphthalene), 141.0 (C4a-naphthalene), 142.9 (C8a-naphthalene), 145.3 (C2-naphthalene), 162.1 (C=O, COOH), 167.8 (C=O), 191.1 (C=S); Anal. Calcd. for $C_{15}H_{11}N_3O_3S_2$: C, 52.16; H, 3.21; N, 12.17; O, 13.90; S, 18.56; Found: C, 52.56; H, 3.51; N, 12.47; S, 18.75.

2.2.4. 5-(Naphthalen-2-Yldiazenyl)-2-Thioxothiazolidin-4-One (4c)

Dark red powder; yield 84%; mp 106 °C; R_f 0.53; IR (KBr, cm^{-1}): 3430 (NH), 3063 (C–H aromatic), 2811 (C–H aliphatic), 1704 (C=O), 1629 (C=C), 1487 (N=N), 1253, 1171 (C=S); ^{1}H-NMR [DMSO-d_6, 400 MHz]: (δ, ppm) 3.76 (brs, 1H, CH), 7.35–8.90 (m, 7H, ArH), 11.38 (brs, 1H, NH, exchanges with D_2O); ^{13}C-NMR [DMSO-d_6, 100 MHz]: (δ, ppm) 109.9 (C5-rhodanine), 116.2 (C3-naphthalene), 122.9 (C1-naphthalene), 125.0 (C7-naphthalene), 126.6 (C6-naphthalene), 129.9 (C4-naphthalene), 130.3 (C8-naphthalene), 134.1 (C5-naphthalene), 141.2 (C4a-naphthalene), 142.9 (C8a-naphthalene), 145.7 (C2-naphthalene), 165.3 (C=O), 206.5 (C=S); Anal. Calcd. for $C_{13}H_9N_3OS_2$: C, 54.34; H, 3.16; N, 14.62; O, 5.57; S, 22.31; Found: C, 54.74; H, 3.18; N, 14.90; S, 22.52.

2.3. Selectivity Studies for Metal Ions Using UV–Vis Spectroscopy

Stock solutions of the metal perchlorates (1.5×10^{-3} M) and rhodanine based azo dyes **4a–c** (5.0×10^{-4} M) were prepared in DMF. The selectivity of azos **4a–c** was studied with various metal ions (including Co^{2+}, Cu^{2+}, Zn^{2+}, Ni^{2+}, and Fe^{3+}) using UV–vis spectroscopy. Spectra of azos **4a–c** (2.50×10^{-5} M, 3000 μL) were recorded in the absence and the presence of four equivalents of metal-ion perchlorate (200 μL, 1.50×10^{-3} M). The solutions were shaken and then incubated for 3 min before scanning at room temperature. UV–vis absorption spectra of the solutions were recorded against DMF. Azo 3 showed selectivity toward Fe^{3+}, therefore, the following experiments were conducted on azo 3 and iron (III) ions.

2.4. UV/Vis and Fluorescence Titration

The interaction between azo **4c** and Fe^{3+} was studied using UV/Vis and fluorescence spectrometry in DMF. Azo **4c** (2.50×10^{-5} M, 3000 μL) in DMF was titrated with iron (III) perchlorate (1.50×10^{-3} M) using UV/vis spectrophotometer and a 1 cm path-length cuvette. After each addition, the solution was shaken and then incubated for 3 min before scanning at room temperature. UV–vis absorption spectra of the solutions were recorded against DMF. Furthermore, the interaction between azo **4c** and the Fe^{3+} was studied using fluorescence spectroscopy. Azo **4c** (2.50×10^{-5} M, 3000 μL) was titrated with successive amounts of iron (III) perchlorate (1.50×10^{-3} M) at the same conditions.

2.5. Binding Stoichiometry Determination

The molar ratio method [17] was used in order to determine the binding stoichiometry of azo **4c** with Fe^{3+}. Azo **4c** (2.50×10^{-5} M, 3000 μL) in DMF was titrated with iron (III) perchlorate (1.50×10^{-3} M) using UV/vis spectrophotometer and a 1 cm path-length cuvette. After each addition, the solution was shaken and then incubated for 3 min before scanning at room temperature. The relation between [Fe^{3+}]/[azo **4c**] against the obtained absorbance of azo **4c** at 396 nm was generated.

2.6. Association Constant Determination

The association constant, *Ka*, for azo **4c** with Fe^{3+} was calculated using the Benesi–Hildebrand equation [18]. Azo **4c** (2.50×10^{-5} M, 3000 µL) in DMF was titrated with iron (III) perchlorate (1.50×10^{-3} M) using UV/vis spectrometry. The solution was shaken then incubated for 3 min before scanning at room temperature. *Ka* was calculated using Equation (1):

$$\frac{1}{A - A_o} = \frac{1}{\left\{ Ka(A_{max} - A_o)[Fe^{3+}]^2 \right\}} + \frac{1}{(A_{max} - A_o)}, \tag{1}$$

where A_o is the absorbance of the receptor (azo **4c**) in the absence of the guest (Fe^{3+}), *A* is the absorbance of azo **4c** after subsequent additions of the guest (Fe^{3+}), A_{max} is absorbance of azo **4c** in the presence of $[Fe^{3+}]_{max}$, and *Ka* is the association constant (M^{-1}). By plotting $1/[Fe^{3+}]^2$ against $1/(A - A_o)$, *Ka* could be determined from the slope of the resulting linear plot.

2.7. Detection Limit (LOD) Determination

The detection limit of azo **4c** for Fe^{3+} was calculated based on IUPAC 3σ criteria using UV/vis spectrophotometer with a 1 cm path-length cuvette. A blank solution of azo **4c** (2.50×10^{-5} M, 3000 µL) in DMF was scanned for at least five times to determine the standard deviation of the blank. The same solution was then titrated with iron (III) perchlorate (1.50×10^{-3} M). After each addition, the solution was shaken and then incubated for 3 min before scanning at room temperature.

A linear calibration curve was established by plotting the absorbance against the concentration of Fe^{3+} ions. The LOD was calculated using Equations (2) and (3):

$$LOD = 3\sigma, \tag{2}$$

$$\sigma = SD/s, \tag{3}$$

where SD is the standard deviation of the blank azo **4c** solution and s is the slope of the calibration curve.

2.8. Antibacterial Activity

The antibacterial activity of **4a–c** was investigated using the antibacterial agar well diffusion assay [19]. Mueller–Hinton agar was prepared by mixing 38.0 g of the agar with 1000 mL of distilled water, then autoclaved. The agar was distributed into the petri dishes and left to solidify at room temperature. The bacterial strains (106 cells/mL) were spread on the agar using pipettes and hockey sticks. Fifty microliters of the examined azo dyes were added separately into the wells and then incubated at 37 °C for 24–48 h. The diameter of the inhibition zone (mm) was measured using a transparent scale in order to determine the bacterial inhibition. The results were compared with the antibiotic amoxicillin (5.0 mg/mL) as a positive control at 50 µL/well.

2.8.1. Test Microorganisms

The activities of azos **4a–c** were studied against *Bacillus pumilus* (NCIM 2189), *Escherichia coli* (NCIM 2343), *Pseudomonas aeruginosa* (NCIM 2863), and *Staphylococcus aureus* (NCIM 2127). The bacterial strains were obtained from the Institute of Microbial Technology, Chandigarh. The bacterial cultures were maintained on nutrient agar slants and stocked as glycerol stocks at −20 °C.

2.8.2. Minimum Inhibitory Concentration (MIC)

The minimum inhibitory concentrations (MIC) of azos **4a–c** were investigated based on the reported protocol by Sarker et al. [20]. A sterile 96-well U-shaped microtiter plate was used to determine the MIC. Double strength Luria Bertani (LB) broth (100 µL) was added into each well of the plate. One hundred microliters of stock solutions of azos **4a–c** were added separately into the first

well of each row and mixed thoroughly. Serial dilutions were made for these solutions in the wells using nutrient broth. One OD_{600} (absorbance of a sample measured at a wavelength of 600 nm) of bacterial suspensions was prepared in Luria Bertani broth, then 10 μL of such suspensions was added to each well and then incubated at 37 °C for 18 h. Resazurin was used to estimate the viable organisms, which convert its color from blue into pink color. MIC is the lowest concentration of the compound that inhibits the growth of the organisms.

3. Results and Discussion

3.1. Synthesis

This research includes the design of new derivatives for naphthalene azo compounds bearing a rhodanine ring with different N-substituents (–NH$_2$, –CH$_2$COOH, and –H) (Figure 1). Diazonium salt of 2-aminonapthalene was prepared by reaction of 2-aminonapthalene with sodium nitrite in the presence of hydrochloric acid. Then this compound was used to prepare the azo derivatives in the presence of sodium acetate. Rhodanine based azo dyes **4a–c** were obtained with a good yield percentage (81%–89%) according to Scheme 1.
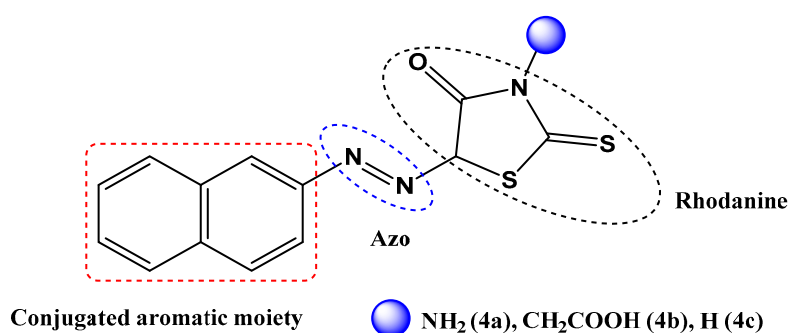

Figure 1. Template design for 5-arylazorhodanine **4a–c**.

Compound	R	% Yield
4a	NH$_2$	81
4b	CH$_2$COOH	89
4c	H	84
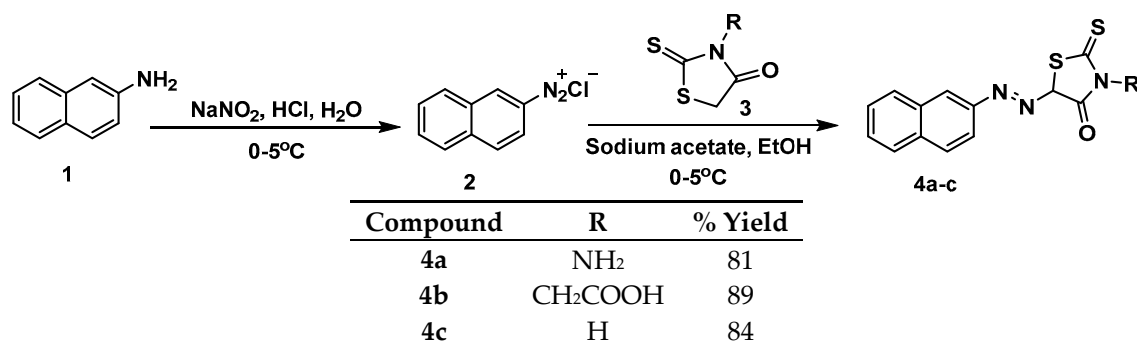
Scheme 1. Synthesis of azo dyes based on rhodanine **4a–c**.

All of the newly synthesized compounds **4a–c** were characterized by IR, ^{1}H NMR, ^{13}C NMR, and elemental analysis. Spectroscopic data were in full agreement with the expected results. Compound **4b** has a dark brown color with a melting point of 130 °C. In the IR spectra of compound **4b**, peaks were seen around 1720 cm^{-1} attributable to the corresponding C=O bond and 1287 cm^{-1} attributable to C=S bond stretching. In addition, the appearance of a new band around the 1403 cm^{-1} region attributed to azo N=N bond stretching in the IR spectra of the compounds **4b** confirmed the completion of the reactions. ^{1}H-NMR spectra for compounds **4b** showed that the signal appeared at δ = 11.69 ppm, which exchanged with D$_2$O assigned for the hydroxy group. The broad singlet appeared at δ = 3.41 ppm corresponding to the H5-rhodanine and integrated into one proton. A multiple signal resonated at δ = 7.36 − 8.79 ppm and, integrated into 7 protons, was assigned to naphthalene protons. The ^{13}C-NMR

showed that the rhodanine C5 resonated at δ = 110.5 ppm. While, the two carbonyl groups appeared at δ = 167.8 and δ = 162.1 ppm and the (C=S) resonated at δ = 191.1 ppm. The elemental analysis for compound **4b** was in agreement with the calculated values as follow: C, 52.56; H, 3.51; N, 12.47; S, 18.75.

3.2. Spectroscopic Analysis

3.2.1. Response Time of Azos **4a–c** for Metal Ions

The sensitivity of azos **4a–c** toward the examined metal ions was evaluated by determining the response time of these compounds toward metal ions in solution. A complex of azos **4a–c** (2.5×10^{-5} M) and four equivalents of each metal ion in DMF was prepared separately and the change in the absorbance intensity of azos **4a–c** was recorded over time. Furthermore, the response time of azo **4c** toward iron (III) ion was estimated using fluorescence spectrometry at the same conditions. The absorbance intensities of azos **4a–c** and the fluorescence intensity of azo **4c** were changed rapidly after adding the metal ion and stabilized after 3 min. The obtained results indicated that azos are sensitive for the examined metal ions therefore, a 3 min incubation time was used in the subsequent experiments to ensure sufficient time for the interaction between the azos and the metal ions.

3.2.2. Colorimetric Sensing and UV/Vis Studies

The interactions between azos **4a–c** and a variety of metal ions (Co^{2+}, Cu^{2+}, Zn^{2+}, Ni^{2+}, and Fe^{3+}) as their perchlorate salt in DMF was studied using colorimetric and UV–vis spectroscopy. Azos **4a–c** (2.5×10^{-5} M) were mixed separately with four equivalents of each metal ion in DMF. The solutions were mixed thoroughly and left to stand for 15 min, then the color change was recorded. When metal ions were added to azo **4a** solution, its color changed from light pink into more intensive color in the case of Zn^{2+} and Ni^{2+} and into yellow color in the case of Co^{2+}, Cu^{2+}, and Fe^{3+} as shown in Figure 2a (S10, Supplementary File). The color change indicated that azo **4a** is sensitive for all metal ions. In the case of azo **4b** solution, its color slightly changed from red into reddish brown/pink color upon addition of metal ions, as shown in Figure 2b (S11, Supplementary File), indicating that azo **4b** is sensitive for all metal ions as well. Figure 2c (S12, Supplementary File) shows that addition of Co^{2+}, Cu^{2+}, and Ni^{2+} did not induce any apparent color change of the yellow color of azo **4c**. Addition of Zn^{2+} caused a slight color change of azo **4c** (light brown), while addition of Fe^{3+} induced a reasonable color change (brown). These results indicated that azo **4c** can serve as a potential candidate for a colorimetric chemosensor of Fe^{3+}.
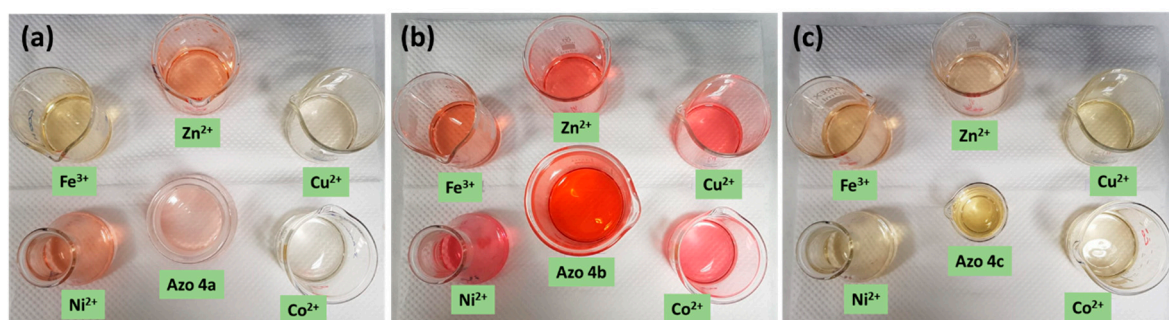

Figure 2. Color change of azo **4a** (**a**), azo **4b** (**b**) and azo **4c** (**c**) (2.5×10^{-5} M) upon addition of four equivalents of different metal ions.

The total color change (ΔE) between azo–metal complexes and the azo dyes (control) was calculated by following equation [21]:

$$\Delta E_{ab} = \sqrt{\left(L^{*} - L_{o}^{*}\right)^{2} + \left(a^{*} - a_{o}^{*}\right)^{2} + \left(b^{*} - b_{o}^{*}\right)^{2}} \tag{4}$$

where L^* and L_o^* are the lightness of azo and its metal complex, respectively; a^* and a_o^* are redness of azo and its metal complex, respectively; b^* and b_o^* are yellowness of azo and its metal complex, respectively.

The total color change ΔE is the distance or the difference between two colors and it is a metric understanding how the human eye perceives color difference. Color change ΔE values more than 3 indicate that the color change is visually perceivable by the human eye [22]. All samples exhibited a color difference value of more than 10.0 as shown in the S13 (Supplementary File), indicating that the color of these samples is noticeably discernable.

Furthermore, to achieve in-depth analysis of the selectivity of azos **4a–c** for metal ions, the change in UV–vis spectra of azos **4a–c** (2.5×10^{-5} M) was investigated upon the addition of four equivalents of the investigated metal ions. Upon the addition of four equivalents of metal ions (Figure 3a), the absorbance of the main band of azo **4a** at 498 nm increased with a small blue shift to 493 nm in the case of Zn^{2+} and 495 nm in the case of Ni^{2+}. This band completely disappeared in the case of Cu^{2+} and Co^{2+} and a shoulder was formed in the case of Fe^{3+}. These results are consistent with the results obtained from the colorimetric investigations indicating that azo **4a** is sensitive to all metal ions. Addition of Co^{2+} and Ni^{2+} to azo **4b** induced a small blue shift from 507 to 503 and 504 nm, respectively, without a change in the band shape as shown in Figure 3b. A strong decrease in the absorbance of azo **4b** occurred after the addition of Fe^{3+} with a small blue shift into 503 nm and a new band was formed at 435 nm indicating that a new complex was formed. Similarly, Zn^{2+} and Cu^{2+} induced a small blue shift into 500 and 503 nm, respectively, and a new shoulder was formed at 435 nm indicating the formation of a new compound. These results showed that azo **4b** is sensitive to all ions; therefore, azo **4a** and azo **4b** could not be used as a selective probe for any of the investigated metal ions. Unlike azo **4a** and azo **4b**, metal ions except Fe^{3+} did not show significant changes in the absorbance intensity, band shift, or band shape of azo **4c** bands. These results indicated that the investigated ions did not show considerable interaction with azo **4c**. Addition of four equivalents of Fe^{3+} caused an increase of the absorbance of azo **4c** bands without any shift in the peak position, as shown in Figure 3c. These results in addition to the significant color change of azo **4c** upon addition of Fe^{3+} indicated that the presence of other cations does not interfere significantly with the binding of azo **4c** toward Fe^{3+} ions in comparison to azos **4a** and **4b**.
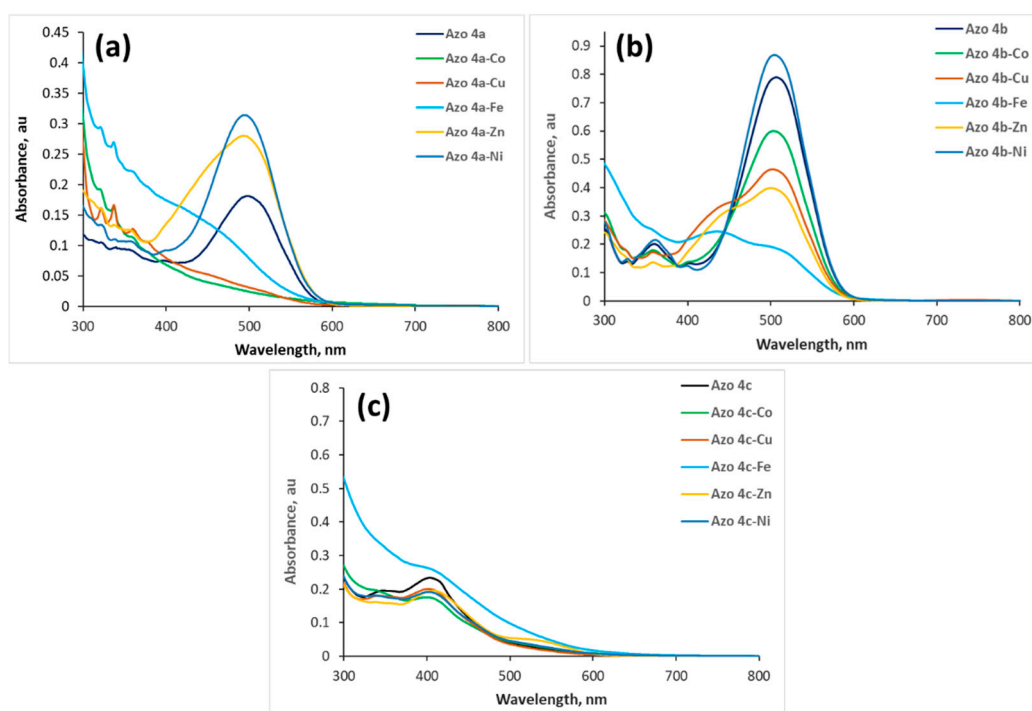
**Figure 3.** UV–vis spectra of azos **4a** (**a**), **4b** (**b**), and **4c** (**c**) (2.5×10^{-5} M) upon addition of four equivalents of different metal ions.

The interaction between azos **4a–c** and metal ions is explained using the interaction between azo **4c** and Fe^{3+} in DMF as an example. UV/vis spectrum of azo **4c** showed main absorbance band at 403 nm with molar absorptivity 9360 M^{-1} cm^{-1} which may be attributed to the π–π^* transition as shown in Figure 4a. The other transition, n–π^*, could not be significantly identified. In general, azobenzene shows two bands: the high intense band appears at ca 350 nm and is attributed to π–π^* transition while the other band, attributed to n–π^* transition, has low intensity (appears at 440 nm) and is not easy to perceive [23]. When azo **4c** was mixed with four equivalents of Fe^{3+}, an increase of the absorbance of the main band was observed without shift in the peak position and without a change of the peak shape as shown in Figure 4a indicating the direct interaction between Fe^{3+} and azo **4c** without affecting its structure.
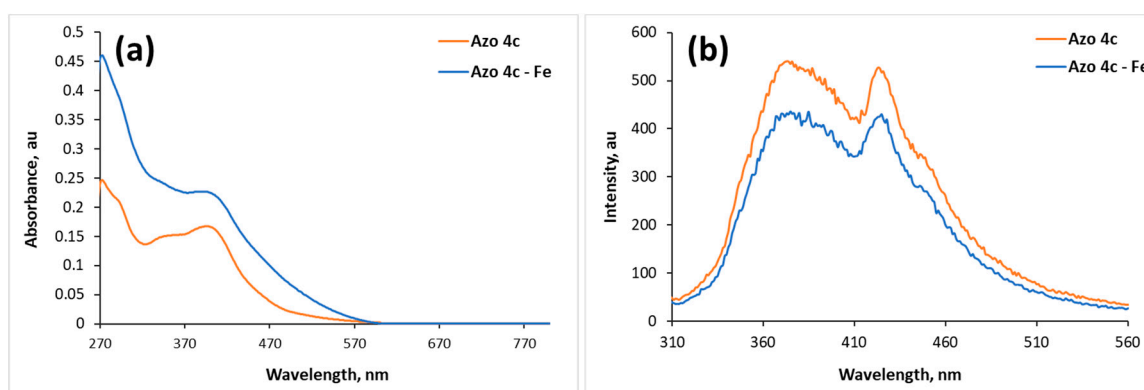
Figure 4. UV/vis absorption spectra of (**a**) azo **4c** (2.5×10^{-5} M) and (**b**) fluorescence spectra of azo **4c** (2.5×10^{-5} M) in the absence and presence of Fe^{3+} (4 equiv.) in DMF.

In addition, the interaction between azo **4c** and Fe^{3+} was studied using fluorescence spectrometry. The emission spectrum of azo **4c** showed two significant bands at 374 and 423 nm when excited at

395 nm. Fluorescence intensity of azo **4c** was quenched upon addition of Fe^{3+} without shift in its peak position as shown in Figure 4b. Ions with a paramagnetic nature such as Fe^{3+} have the ability to quench the fluorescence intensity of a fluorophore through photoinduced metal-to-fluorophore electron transfer or electronic energy transfer mechanisms [24,25]. It is reported that Fe^{3+} ion is a well-known efficient fluorescence quencher because of its paramagnetic properties via electron or energy transfer [26]. Iron (III) has been proved to preferentially bind with the nitrogen atom of imino group and oxygen atom of carbonyl group [16,27]. Therefore, we think that Fe^{3+} could accept electrons from the nitrogen atom of imino group and oxygen atom of carbonyl group in azo **4c** molecule, since Fe^{3+} is six-coordinated and it has unoccupied sites which might be occupied by other azo molecules. Consequently, intra-particle cross-links are induced by the produced coordination interactions causing a quenching in the fluorescence intensity [28] as shown in Figure 5.
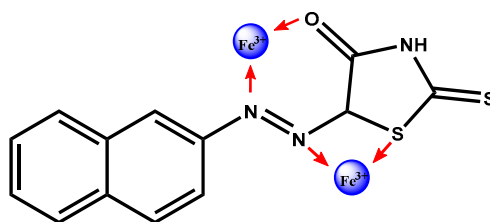
Figure 5. The suggested azo **4c**–iron (III) complex structure.

3.2.3. Binding Stoichiometry

The complexation ratio of azo **4c** with Fe^{3+} was investigated using the molar ratio method. Azo **4c** was titrated with Fe^{3+} in DMF using UV–vis spectrometry. A plot of $[Fe^{3+}]/[azo\ 4c]$ versus the absorbance of azo **4c** at 398 nm was generated. The stoichiometric ratio between azo **4c** and Fe^{3+} was found to be 1:2 as shown in Figure 6 (S14, Supplementary File) indicating that the formed complex has an M_2L structure. These results are reasonable because azo **4c** has two binding sites.
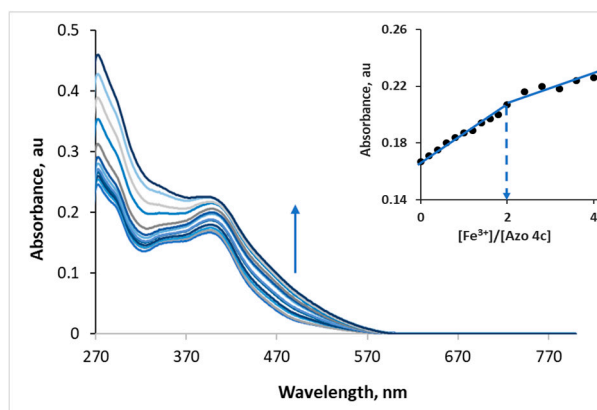

Figure 6. UV/vis titration of azo **4c** (2.5×10^{-5} M) with Fe^{3+} (1.5×10^{-3} M) in DMF. Inset: Molar ratio method for determination of the binding stoichiometry of azo **4c** with Fe^{3+} (4 equiv.).

3.2.4. Association Constant

To get further insight into the bindings between azo **4c** and Fe^{3+}, the binding affinity of Fe^{3+} toward azo **4c** was investigated using the Benesi–Hildebrand equation based on a 1:2 stoichiometric ratio (Equation (1)). Figure 7 shows a good linearity with correlation coefficient of $R^2 = 0.9896$ and linear regression equation of $y = 3 \times 10^{-8}x + 13.206$ for azo **4c**. The linearity of the obtained plot indicated that stoichiometry for azo **4c** with Fe^{3+} was 1:2. These results are consistent with the results observed using the molar ratio method [29]. The calculations showed high association constant of azo **4c** to Fe^{3+} as 4.63×10^8 M^{-1} indicated that Fe^{3+} showed high binding affinity toward azo **4c** comparable

with reported receptors that show high selectivity toward Fe^{3+} [30,31]. For instance, rhodamine B with thiocarbonyl moieties showed a binding constant of 2.75×10^4 M^{-1} [32], another rhodamine B derivative showed 1.52×10^4 M^{-1} [33]. Furthermore, azo-Schiff base receptors containing azo and azomethine groups showed $7.72 \times 10^4 - 1.21 \times 10^5$ M^{-1} [33].
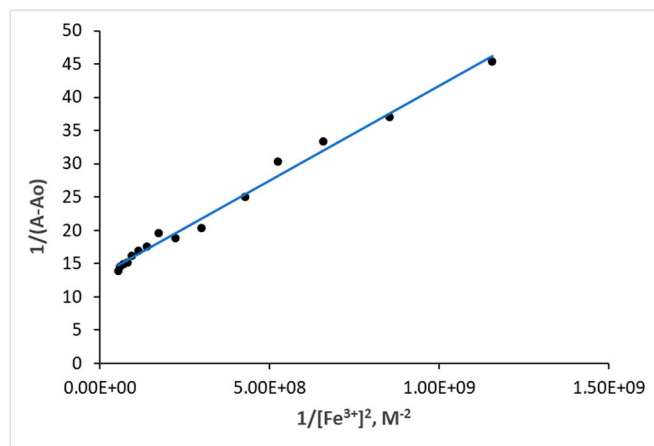
Figure 7. Benesi–Hildebrand plot for the 1:2 binding stoichiometry of azo **4c** with Fe^{3+}.

3.2.5. Detection Limit

The detection limit (LOD) of azo **4c** for Fe^{3+} was calculated using Equations (2) and (3) based on UV/vis calibration curve. The LOD of azo **4c** for Fe^{3+} was found to be 5.14 µM as shown in Figure 8, indicating that azo **4c** showed significant sensitivity for Fe^{3+}. Our azo probe showed an acceptable value in comparison with some of the previous reports on the Fe^{3+} chemosensors in terms of their LOD values. For instance, 1,10-phenanthroline complexes showed an LOD of 1.61×10^{-5} M [34], while azo-Schiff base receptors containing azo and azomethine groups showed an LOD of 6.44×10^{-6} M [31].
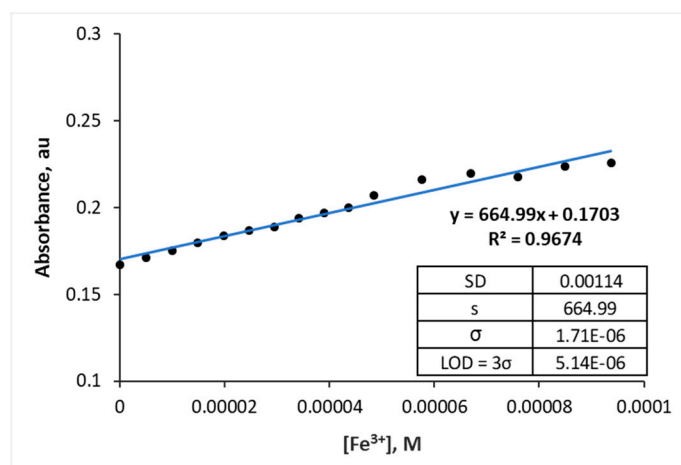
Figure 8. Calibration curve for the absorbance of azo **4c** as a function of $[Fe^{3+}]$.

3.3. Biological Studies

Antimicrobial Activity

Biological activities of the compounds containing rhodanine azos **4a–c** have stimulated great interest to explore the synthesis of new and potentially useful compounds. The antibacterial activities of rhodanine azos **4a–c** were evaluated in vitro against one gram-positive bacterial strain namely, *S. aureus* (NCIM 2127); and two gram-negative bacterial strains namely, *E. coli* (NCIM 2343) and

P. aeruginosa (NCIM 2863) using the well diffusion method. The results were compared with amoxicillin as a reference standard. The results of the obtained derivatives **4a–c** are summarized in Table 1. Compounds **4a–c** showed a good activity against both gram-positive and gram-negative bacteria compared with amoxicillin. The in vitro antibacterial screening of compounds **4a–c** against *E. coli* showed that compound **4c** (MIC = 0.625 µg/mL) exhibited a good antibacterial activity compared with the standard compound (amoxicillin's MIC = 0.1 µg/mL) whereas compounds **4a** and **4b** showed an MIC value of 2.5 and 1.25 µg/mL respectively. Compounds **4a** and **4b** were found to inhibit *P. aeruginosa* at MIC values of 2.5 µg/mL. The remaining compound **4c** showed no activity against *P. aeruginosa*. In addition, all compounds **4a–c** exhibited good antimicrobial activities against gram-positive bacteria *S. aureus* strain with an MIC ranging between 1.25 and 2.5 µg/mL, where the reference compound (amoxicillin) showed no activity. Therefore, by evaluating the obtained biological results for the novel azo rhodanine analogues, **4a–c** showed a good antibacterial activity against both gram-positive and gram-negative bacteria (Table 1). The structure–activity relationship (SAR) studies of our compounds revealed that the compounds with an acetyl group at the *N*-rhodanine ring contributed to a better antibacterial activity than those with amino or free *N*-rhodanine.

Table 1. Agar well diffusion method–zone of inhibition and minimum inhibitory concentration (MIC, µg/mL) of rhodanine azos **4a–c**.

Compounds	Zone of Inhibition (cm) *			MIC (µg/mL)		
	E. coli	*P. aeruginosa*	*S. aureus*	*E. coli*	*P. aeruginosa*	*S. aureus*
4a	0.7	0.9	0.8	2.5	2.5	2.5
4b	0.9	1.0	0.7	1.25	2.5	1.25
4c	0.6	NA	1.0	0.625	NA	1.25
Amoxicillin	0.8	2.2	NA	0.1	0.0125	NA

* An error value of 0.1–0.05 cm can be expected.

4. Conclusions

In summary, we have reported the synthesis of three rhodanine azo compounds. On the basis of the obtained results from the antibacterial test, compounds **4b** showed a moderate growth-inhibitory effect against all tested bacteria. Among the compounds, **4c** exhibited the most antibacterial activity against *E. coli*. UV/vis and fluorescence analyses confirmed the interaction between azos **4a–c** and metal ions. However, azo **4c** showed high selectivity and sensitivity for Fe^{3+} with a binding constant of 4.63×10^8 M^{-1} and an LOD of 5.14 µM and with 1:2 stoichiometry. We believe that these results are sufficiently promising to conduct further studies into the development of rhodanine-based azo dye chemosensors for Fe^{3+} in various environmental and biological systems.

References

1. Chen, H.; Cho, C.; Wan, F.; Wu, T. A colorimetric sensor for Fe^{2+} ion. *Inorg. Chem. Commun.* **2014**, *41*, 88–91. [CrossRef]

2. El-Kady, A.A.; Abdel-Wahhab, M. Occurrence of trace metals in foodstuffs and their health impact. *Trends Food Sci. Technol.* **2018**, *75*, 36–45. [CrossRef]

3. Khalid, S.; Shahid, M.; Natasha, B.I.; Sarwar, T.; Shah, A.H.; Niazi, N.K. A review of environmental contamination and health risk assessment of wastewater use for crop irrigation with a focus on low and high-income countries. *Int. J. Environ. Res. Public Health.* **2018**, *15*, 895. [CrossRef]

4. Rull-Barrull, J.; d'Halluin, M.; Le Grognec, E.; Felpin, F.X. Chemically-modified cellulose paper as smart sensor device for colorimetric and optical detection of hydrogen sulfate in water. *Chem. Commun.* **2016**, *52*, 2525–2528. [CrossRef] [PubMed]

5. Khedr, A.M.; Saad, F.A. Synthesis, structural characterization, and antimicrobial efficiency of sulfadiazine azo-azomethine dyes and their bi-homonuclear uranyl complexes for chemotherapeutic use. *Turk. J. Chem.* **2015**, *39*, 267–280. [CrossRef]

6. Refat, M.S.; El-Sayed, M.Y.; Adam, A.M.A. Cu (II), Co (II) and Ni (II) complexes of new Schiff base ligand: Synthesis, thermal and spectroscopic characterizations. *J. Mol. Struct.* **2013**, *1038*, 62–72. [CrossRef]

7. Kadhum, A.A.H.; Al-Amiery, A.A.; Musa, A.Y.; Mohamad, A.B. The antioxidant activity of new coumarin derivatives. *Int. J. Mol. Sci.* **2011**, *12*, 5747–5761. [CrossRef]

8. Bayindir, S. A simple rhodanine-based fluorescent sensor for mercury and copper: The recognition of Hg^{2+} in aqueous solution, and Hg^{2+}/Cu^{2+} in organic solvent. *J. Photoch. Photobio. A* **2019**, *372*, 235–244. [CrossRef]

9. Lohani, C.R.; Lee, K.H. The effect of absorbance of Fe^{3+} on the detection of Fe^{3+} by fluorescent chemical sensors. *Sens. Actuators B Chem.* **2010**, *143*, 649–654. [CrossRef]

10. Wang, C.; Zhang, D.; Huang, X.; Ding, P.; Wang, Z.; Zhao, Y.; Ye, Y. A fluorescence ratiometric chemosensor for Fe^{3+} based on TBET and its application in living cells. *Talanta* **2014**, *128*, 69–74. [CrossRef]

11. Ghaedi, M.; Mortazavi, K.; Montazerozohori, M.; Shokrollahi, A.; Soylak, M. Flame atomic absorption spectrometric (FAAS) determination of copper, iron and zinc in food samples after solid-phase extraction on Schiff base-modified duolite XAD 761. *Mater. Sci. Eng. C Mater. Biol. Appl.* **2013**, *33*, 2338–2344. [CrossRef] [PubMed]

12. Mustafa, Y.F. Synthesis of new coumarin derivatives with suspected anticoagulant activity. *Iraqi J. Pharm. Sci.* **2012**, *12*, 20–32. [CrossRef]

13. Liu, X.; Li, N.; Xu, M.-M.; Wang, J.; Jiang, C.; Song, G.; Wang, Y. Specific colorimetric detection of Fe^{3+} ions in aqueous solution by squaraine-based chemosensor. *RSC Adv.* **2018**, *8*, 34860–34866. [CrossRef]

14. Bobrowski, A.; Nowak, K.; Zarebski, J. Application of a bismuth film electrode to the voltammetric determination of trace iron using a Fe(III)-TEA-BrO_3- catalytic system. *Anal. Bioanal. Chem.* **2005**, *382*, 1691–1697. [CrossRef] [PubMed]

15. Sil, A.; Ijeri, VS.; Srivastava, AK. Coated-wire iron(III) ion-selective electrode based on iron complex of 1,4,8,11-tetraazacyclotetradecane. *Sens. Actuators B Chem.* **2005**, *106*, 648–653. [CrossRef]

16. Lee, M.H.; Giap, T.V.; Kim, S.H.; Lee, Y.H.; Kang, C.; Kim, J.S. A novel strategy to selectively detect Fe(III) in aqueous media driven by hydrolysis of a rhodamine 6G Schiff base. *Chem. Commun.* **2010**, *46*, 1407–1409. [CrossRef]

17. Marcus, Y. On the Use of the Molar Ratio Method for Determining Association Stoichiometry. *Isr. J. Chem.* **1967**, *5*, 143–149. [CrossRef]

18. Benesi, H.A.; Hildebrand, J. A spectrophotometric investigation of the interaction of iodine with aromatic hydrocarbons. *J. Am. Chem. Soc.* **1949**, *71*, 2703–2707. [CrossRef]

19. AlNeyadi, S.S.; Salem, A.A.; Ghattas, M.A.; Atatreh, N.; Abdou, I.M. Antibacterial activity and mechanism of action of the benzazole acrylonitrile-based compounds: *In vitro*, spectroscopic, and docking studies. *Eur. Eur. J. Med. Chem.* **2017**, *136*, 270–282. [CrossRef]

20. Sarker, S.D.; Nahar, L.; Kumarasamy, Y. Microtitre plate-based antibacterial assay incorporating resazurin as an indicator of cell growth, and its application in the in vitro antibacterial screening of phytochemicals. *Methods* **2007**, *42*, 321–324. [CrossRef]

21. Barreiro, J.; Milano, M.; Sandoval, A. Kinetics of colour change of double concentrated tomato paste during thermal treatment. *J. Food Eng.* **1997**, *33*, 359–372. [CrossRef]

22. Noh, H.L.; Park, Y.K.; Oh, B.M.; Zheng, J.; Kim, S.-H.; Lee, W.; Jong, H.K. Colorimetric chemosensor for detection of a volatile organic compound, ethylamine, under versatile conditions: Solution, thin-film, and dyed fabric. *Sens. Actuators B Chem.* **2019**, *301*, 127079. [CrossRef]

23. Natansohn, A.; Rochon, P. Photoinduced motions in azo-containing polymers. *Chem. Rev.* **2002**, *102*, 39–76. [CrossRef] [PubMed]

24. Pal, S.; Chatterjee, N.; Bharadwaj, P.K. Selectively sensing first-row transition metal ions through fluorescence enhancement. *RSC Adv.* **2014**, *4*, 26585–26620. [CrossRef]

25. Varnes, A.W.; Dodson, R.B.; Wehry, E. Interactions of transition-metal ions with photoexcited states of flavines. Fluorescence quenching studies. *J. Am. Chem. Soc.* **1972**, *94*, 946–950. [CrossRef]

26. Li, J.; Wang, Q.; Guo, Z.; Ma, H.; Zhang, Y.; Wang, B.; Bin, D.; Wei, Q. Highly selective fluorescent chemosensor for detection of Fe^{3+} based on Fe_3O_4@ZnO. *Sci. Rep.* **2016**, *6*, 23558–23566. [CrossRef]

27. Weerasinghe, A.J.; Abebe, F.A.; Sinn, E. Rhodamine based turn-ON dual sensor for Fe^{3+} and Cu^{2+}. *Tetrahedron Lett.* **2011**, *52*, 5648–5651. [CrossRef]

28. Yuan, X.; Luo, Z.; Yu, Y.; Yao, Q.; Xie, J. Luminescent noble metal nanoclusters as an emerging optical probe for sensor development. *Chem. Asian J.* **2013**, *8*, 858–871. [CrossRef]

29. Shiraishi, Y.; Sumiya, S.; Kohno, Y.; Hirai, T. A Rhodamine−cyclen conjugate as a highly sensitive and selective fluorescent chemosensor for Hg(II). *J. Org. Chem.* **2008**, *73*, 8571–8574. [CrossRef]

30. Kaur, K.; Chaudhary, S.; Singh, S.; Mehta, S.K. Highly selective probe based on imine linkage for Zn^{2+} and HSO_3^- in mixed aqueous media. *J. Lumin.* **2015**, *160*, 282–288. [CrossRef]

31. Özdemir, Ö. Synthesis of novel azo linkage-based Schiff bases including anthranilic acid and hexanoic acid moieties: Investigation of azo-hydrazone and phenol-keto tautomerism, solvatochromism, and ionochromism. *Turk. J. Chem.* **2019**, *43*, 266–285. [CrossRef]

32. Fu, Y.; Pang, X.X.; Wang, Z.Q.; Chai, Q.; Ye, F. A highly sensitive and selective fluorescent probe for determination of Cu (II) and application in live cell imaging. *Spectrochim Acta A Mol. Biomol. Spectrosc.* **2019**, *208*, 198–205. [CrossRef] [PubMed]

33. Chen, H.; Bao, X.; Shu, H.; Zhou, B.; Ye, R.; Zhu, J. Synthesis and evaluation of a novel rhodamine B-based 'off-on' fluorescent chemosensor for the selective determination of Fe^{3+} ions. *Sen. Actuators B Chem.* **2017**, *242*, 921–931. [CrossRef]

34. Kozak, L.; Niedzielski, P.; Wachowiak, W. The tandem analytical method of flow injection diode array spectrophotometry and flame atomic absorption spectrometry (FI-DAD(vis)-FAAS) in iron speciation studies using 1,10-phenanthroline complexes. *Microchem. J.* **2013**, *110*, 54–60. [CrossRef]